JOURNAL OF GEOPHYSICAL RESEARCH, VOL. 97, NO. B1, PAGES 479–488, JANUARY 10, 1992

Patterns of Seismic Activity Preceding Large Earthquakes

BRUCE E. SHAW, J. M. CARLSON,[1] AND J. S. LANGER

Institute for Theoretical Physics, University of California, Santa Barbara

We analyze the patterns of seismic activity which precede large events in a mechanical model of a fault. The model generates a statistical distribution of events similar to that observed for a single fault, with a scaling region consistent with the Gutenberg-Richter law at small and moderate magnitudes, and an excess of events at large magnitudes. We find only slight variation in the scaling behavior during a loading cycle. However, we do observe systematic variations in space and time of the overall rate of activity. In the model, the activity accelerates dramatically preceding a large event and is usually a maximum in the neighborhood of the future epicenter. These results are compared to California seismicity data, where we find that activity patterns vary regionally. Looking at patterns of activity in the San Francisco Bay Area since 1948, we find an increase of activity on the Calaveras fault near San Jose beginning in the 1980s which, if our model is relevant, would forecast a large earthquake in that region. The 1989 Loma Prieta earthquake occurred on the San Andreas fault within 30 km of the section of the Calaveras fault showing increased activity.

1. INTRODUCTION

Discovering reliable methods for predicting large earthquakes is difficult because of the infrequency of these events, which have mean recurrence times of the order of 100 years on the most active faults. On the other hand, smaller earthquakes are quite numerous. Thus any information one could deduce from them about large events would be of interest [*Wyss and Habermann*, 1979; *Carlson*, 1991]. In this paper, we study correlations between small and large events for a theoretical model of a fault. We present a series of statistical measurements of activity patterns for the smaller events which precede large ruptures and discuss the relationship of our results to seismological data. In particular, we look at variations in the scaling behavior and activity rates and use these to address specific questions of seismological relevance, including locations of epicenters, preshocks, and quiescence.

We then make a very preliminary attempt to relate these ideas to real data. Looking at patterns of activity in California, we observe that different regions display patterns that are characteristic of those regions and are repeatable for different events. The types of patterns seen are more varied, however, than the generic increase in activity preceding large events in the model. While long-term increases in activity are clearly not a necessary predecessor of large events, the observation of a long-term increase, we believe, is a signal of a coming large event. Looking at earthquakes in the San Francisco Bay Area since 1948, we find patterns of activity that suggest a long-term forecast for a large earthquake on the central Calaveras fault. The 1989 Loma Prieta earthquake on the San Andreas fault was very near this segment of the Calaveras fault and possibly relieved the near-threshold stress suggested by the patterns of activity. If this interpretation is correct, patterns of activity on the central Calaveras fault should change, with the activity dropping. If, instead, after a few years the activity remains high, there may still be a forthcoming large earthquake on this segment. Observations in the next few years should be able to test this.

The model that we use was studied recently by *Carlson and Langer* [1989*a*, 1989*b*] and *Carlson* 1991], and belongs to a class of block and spring models introduced more than 20 years ago by *Burridge and Knopoff* [1967]. The model is of interest as an example of "self-organized criticality" — a class of systems introduced by *Bak, et al.* [1987] which, due to a dynamic threshold instability, generate scale-invariant sequences of events. The importance of the model comes from the fact that, in the absence of spatial inhomogeneities or stochasticity, it dynamically generates a statistical distribution of both large and small slipping events which is consistent with that seen in nature for a single fault. For the smaller events, the magnitude versus frequency distribution $\mathcal{R}(\mu)$ of events of magnitude μ is consistent with the fundamental statistical law, first introduced by *Gutenberg and Richter* [1954], governing the rate of earthquake occurrence:

$$\mathcal{R}(\mu) = Ae^{-b\mu}\,, \tag{1}$$

where A is independent of μ and $b \cong 1$. The large events occur at a rate in excess of the value extrapolated from equation (1), as is seen along certain major faults where sufficient data are available [*Wesnousky, et al.*, 1983; *Davison and Scholz*, 1985; Schwartz and Coppersmith, 1984].

In this paper we present a statistical study of the activity patterns of smaller events, satisfying the Gutenberg-Richter law (equation (1)), which precede large events. In equation (1), the magnitude μ is a logarithmic measure of the size of an event. The parameter b is thus the exponent of the power law relating frequencies of events of different sizes, and the amplitude A is a measure of the activity.

Real earthquakes can be thought of as slipping events on a two-dimensional interface in a three-dimensional inhomogeneous linear elastic medium. The interfaces form a complicated, possibly fractal, network of faults. The friction is some nonlinear stick-slip function of the relative motions of the rocks on opposite sides of the interfaces. Our model, on the other hand, is a one-dimensional interface in a one-dimensional homogeneous linear elastic medium. We study a single, straight, isolated fault. The friction is a nonlinear

[1] Now at Department of Physics, University of California, Santa Barbara.

Paper number 91JB01796.
0148-0227/92/91JB01796$05.00

stick-slip function depending only on the local velocity. The point of studying this model is to see what kind of behavior is exhibited by this stripped down, minimal, dynamical system: How are the features similar to real earthquakes, and how are they different? Where the model does differ, which of the many aspects that we have neglected — the elastic medium being of higher dimensionality than the interface, inhomogeneities, interacting faults, couplings to other physical processes — can we add back in to find a closer correspondence? In this paper we present some patterns of small-event activity during the loading cycle between large events, beginning with the model and then turning to real data along the San Andreas fault in California. The ambitious second question — tracking down the sources of the complexity in the real data — will have to wait for future work.

This paper is organized as follows: In section 2, we present the model, reviewing briefly the features of relevance to the work presented here. In section 3, we present our numerical results on the activity patterns preceding large events in the model. In section 4, we turn to real earthquakes. We present evidence for the long term forecast of a large earthquake on the central Calaveras fault. We then look at patterns of activity from other regions of the San Andreas fault system. Finally, we conclude and summarize our results in section 5.

2. The Model

The model (see Figure 1) consists of a series of identical masses connected to each other by coupling springs of uniform stiffness. Another set of uniform pulling springs connects each block to a fixed plate. The blocks rest on another plate that moves with a small constant velocity relative to the fixed plate and experience a friction force that depends on the velocity of each individual block. The only nonlinearity in the problem is the friction ϕ: a stick-slip, velocity-weakening force (Figure 2). A detailed discussion of the model is given by *Carlson and Langer* [1989*b*].

The dimensionless equation of motion for the chain of harmonic blocks is

$$\ddot{U}_j = \ell^2(U_{j+1} - 2U_j + U_{j-1}) - U_j - \phi(2\alpha(\nu + \dot{U}_j)) \quad (2)$$

where U_j is the displacement of the jth block, and the dots denote differentiation with respect to time τ, scaled so that the period of oscillation of a single block attached only to a pulling spring, with no friction, is 2π. There are three dimensionless parameters in the equation. The parameter describing the rate of velocity weakening in the friction is α,

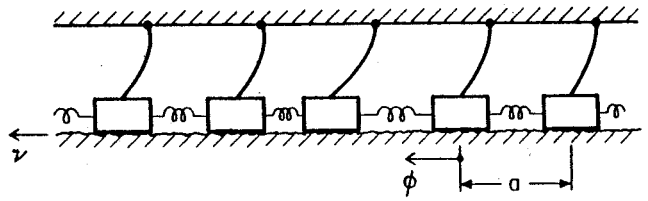

Fig. 1. Theoretical, mechanical model of a fault. The block and spring model consists of a one-dimensional chain of equal masses. Each block is joined to its nearest neighbors by coupling springs of equal strength. Pulling springs of equal strength attach the blocks to a fixed plate. They are in contact with another plate which is moving at constant velocity ν. Between each block and the moving plate there is a friction force ϕ which depends only on the velocity of the block. The equilibrium spacing between the blocks is a.

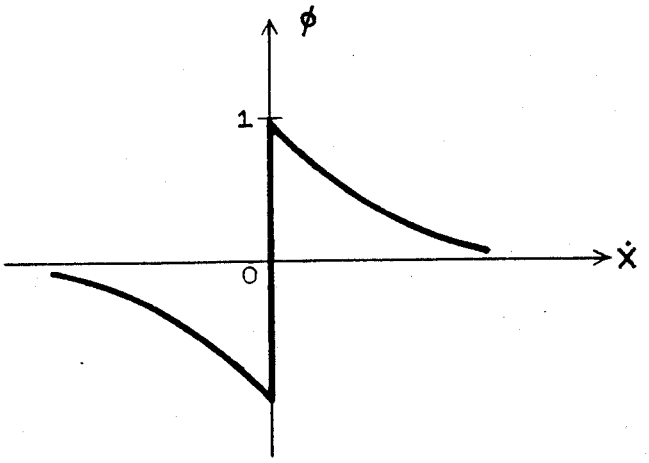

Fig. 2. The velocity-weakening stick-slip friction force $\phi(\dot{x})$, given in equation (3). The friction ϕ depends only on the velocity $\dot{x}$.

which is a particularly important parameter in the dynamics. The ratio of the slipping time to the loading time (i.e., the average time interval between large events) is ν. For real faults, slipping times are of the order of 1 s, and loading times are tens or hundreds of years; thus $\nu \lesssim 10^{-9}$. The ratio of the stiffness of the coupling spring to that of the pulling spring is ℓ^2. The equilibrium spacing between the blocks, a, does not appear explicitly in the equation of motion; however, in the continuum limit, $\xi = \ell a$, is the sound speed. Here we use periodic boundary conditions; however, our results are not sensitive to whether the boundary conditions are free or periodic.

The friction function that we use in numerical solutions of equation (2) is illustrated in Figure 2. When $\dot{x} = 0$ ($\dot{x} = \dot{u}_j + \nu$ is the relative velocity between a block and the moving plate) static friction is in the range ± 1. When $\dot{x} \neq 0$, dynamic friction is given by

$$\phi(2\alpha\dot{x}) = \frac{1}{1 + 2\alpha\dot{x}} \left(\frac{\dot{x}}{|\dot{x}|} \right). \quad (3)$$

The crucial feature of the friction is that it exhibits velocity weakening; i.e., there is a range of velocities for which $d\phi/d\dot{x} < 0$. For this range of velocities, a linear stability analysis shows that all Fourier modes grow exponentially at finite rate, so that inhomogeneities are magnified during slipping. As a consequence of this dynamical instability the deterministic equation (2) generates a noisy chaotic sequence of events.

Given any nonuniform initial condition, the system reaches a statistically steady state within a few cycles of large events. An event occurs when a connected set of blocks undergoes a slipping motion. The corresponding total moment is the sum of the displacements δU_j of the blocks:

$$M = \sum_j \delta U_j, \quad (4)$$

and the magnitude μ is $\mu = \ln(M)$.

A typical magnitude versus frequency distribution $\mathcal{R}(\mu)$ is illustrated in Figure 3. The key features of this distribution are the scaling region ranging from small to moderate values of μ, in which the distribution $\mathcal{R}_S(\mu)$ is consistent with the Gutenberg-Richter law (equation (1)) and the region of large events is described by a separate distribution $\mathcal{R}_G(\mu)$. The large events occur more frequently than would be expected

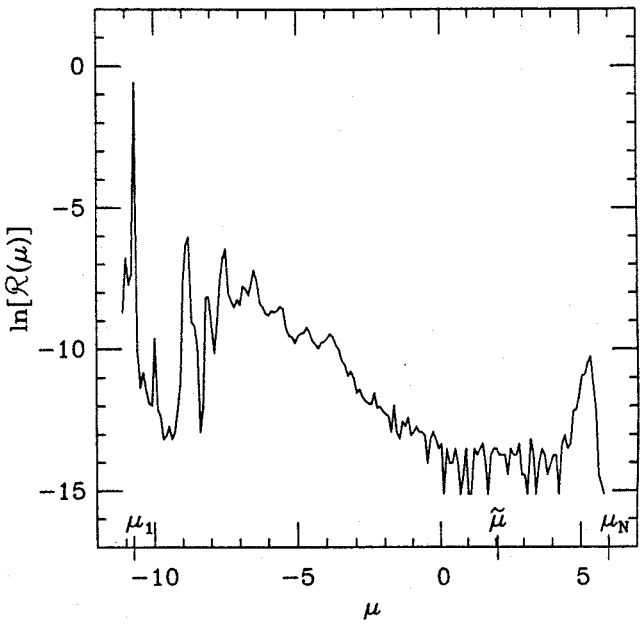

Fig. 3. Rate $\mathcal{R}(\mu)$ of events of magnitude μ. Microscopic one block events have magnitude μ_1. The crossover from the scaling region to the large events peak occurs at $\tilde{\mu} \cong \ln(2\xi/\alpha)$. The largest possible event has magnitude μ_N. The parameters used in this figure are $\alpha = 2.5$, $\xi = 10$, $\nu = 0.01$, and $N = 200$, where N is the number of blocks in the system.

from an extrapolation of the rate of smaller events and account for nearly all of the forward motion of the blocks. The maximum large event that the system can sustain has a moment $M_N(\alpha)$ which scales with the length N of the fault. The crossover from scaling behavior to large events was described analytically by *Carlson and Langer* [1989*b*] and corresponds to an initial triggering zone (i.e., a connected set of blocks which are on the verge of slipping) of length approximately

$$\tilde{\xi} \approx \frac{2\xi}{\alpha} \ln\left[\frac{4\xi l^2}{\nu a}\right], \tag{5}$$

with associated moment $\tilde{M} \approx 2\xi/\alpha$.

It is important to understand that, while this simple deterministic model exhibits a variety of more-or-less realistic phenomena, it has definite limitations. It pertains strictly to a single, isolated, one-dimensional fault with no extrinsic irregularities, bends, or other major asperities. Its only irregularities are self-generated. Moreover, it has no mechanism for generating aftershocks. There is no state dependence of the friction law, nor is there any way for one region of the fault to communicate with another unless all of the blocks in between the two regions come unstuck.

We believe that it is possible, however, that this model can be interpreted as describing some kind of average behavior of an interconnected and only roughly linear system of faults. That is, it may be that this very simplified model provides a crude but in some ways qualitatively accurate picture of the zone of interaction between tectonic plates, giving only roughly localized regions of activity, and not discriminating between main events and their aftershocks. We will not know whether this conjecture has any merit until we can make comparisons between the behavior of this model and observations in the real world. The remainder of this paper contains a report of our first efforts to move in this direction.

3. Patterns of Activity in the Model

We now present a number of results for patterns of smaller events preceding large events in the model. The sequence of events generated by the model is divided into a series of cycles, with each large event marking the end of a cycle. We define a large event to be one for which the moment is larger than $\tilde{M} \approx 2\xi/\alpha$, which is the crossover moment defined in the previous section. As shown by *Carlson* [1991], there is a broad distribution of time intervals between these large events. Here we study the smaller events, looking for information about the forthcoming large event. A central result is that the value of the scaling exponent b in equation (1) does not vary in space and only varies slightly in time. In marked contrast, the prefactor A, the activity, varies in both space and time. The latter variation allows us to track the behavior of all the events in the scaling region by studying the more numerous smaller events.

To study the possible variation of b in space and time, we separate events into different groups depending on how long they happened before the large event and how far they were from the epicenter. We then superimpose the partial distributions $\mathcal{R}(\mu)$ for 1000 large-event cycles. No spatial variation in b is seen for events that occur in a region of size $\tilde{\xi}$ around the future epicenter, as compared to events farther away. The value of b does decrease slightly with time, changing of the order of 20% between the earliest and latest times in the cycle. While on average there is a slight change, for each cycle the noise is much larger than this small signal. Within the context of the model, the use of b values for prediction of upcoming large events does not seem possible, although some cases of significant variation of b values in real earthquakes have been observed. [e.g., *Smith*, 1981].

While b does not vary significantly, A shows strong systematic variations in space and time, not only on average, but also within each cycle. These variations appear to be useful for predictive purposes. Here, we are interested in how A varies in space and time; the actual value of A is unimportant. Therefore instead of trying to measure A directly, we define a weighted activity A_W which is a sum over all the events, with each event weighted by some function of its size. This measure has two advantages. First, the main advantage is that it does not depend on the exact distribution $\mathcal{R}(\mu)$; if it is of the general form given in equation (1), one does not have to know the value of b and, even more generally, the distribution need not even be of this form. A second advantage is that the exact weighting does not matter, as long as the weighting is such that the more numerous small events dominate the sum. We can thus choose the most convenient weighting for a particular application.

The equation expressing this idea is

$$A_W(s,t) = \frac{1}{d_s d_t} \sum_{\substack{\text{events such that:} \\ s < s' < s + d_s \\ t < t' < t + d_t}} W(\text{event}) \tag{6}$$

where for each event, s' denotes the position of the epicenter, t' denotes the time at which it occurred, and W is the weighting of the events (discussed in detail below).

Here, d_s and d_t denote the widths of the intervals in space and time, respectively, into which the events have been

grouped. By summing over events in these intervals and then dividing by the product $d_s d_t$, we obtain a rate per unit length of the fault.

Because the events are separated and distinct in time, it is useful to consider the integrated activity

$$A^{\rm cum}(s,t) = \int_{t^{(0)}}^{t^{(0)}+t} A_W(s,t')dt' \qquad (7)$$

where $t^{(0)}$ is some arbitrary time at which we start counting events. Then the weighted activity is just the slope of the cumulative activity in time: $A_W = dA^{\rm cum}/dt$.

To get the smoothest measure, we choose a weighting so the most numerous smallest events dominate the sum. This weighting should be contrasted with a weighting where events of all sizes contribute, or one where only the largest sizes dominate. For $b = 1$ a weighting by the moment M would have events of all sizes contributing equally to the sum. This would give a noisy signal, with the occasional bigger events dominating the local rate. Therefore we must choose a weighting of events of different sizes which, in the case of $b = 1$, increases less rapidly than the moment.

We find two weightings convenient. In the first we weight all events with magnitudes in a given window equally:

$$W_0(\text{event}) = \begin{cases} 1\ , & \mu_{\rm lower} < \mu < \mu_{\rm upper} \\ 0\ , & \text{otherwise} \end{cases} \qquad (8)$$

Our second choice is to assign to events with magnitudes in the given window weights equal to the numbers of blocks that slipped. That is,

$$W_\Delta(\text{event}) = \begin{cases} \Delta(\text{event})\ , & \mu_{\rm lower} < \mu < \mu_{\rm upper} \\ 0\ , & \text{otherwise} \end{cases} \qquad (9)$$

where Δ(event) is the size of the slip zone for the event, which for the model is simply the number of blocks. For the upper cutoff we use $\mu_{\rm upper} = \tilde{\mu}$ in the model. The lower cutoff is taken to be as small as possible to get the best statistics. For the model, we choose the lower end of the well-defined scaling region. For real earthquakes, we pick the smallest magnitudes that can be uniformly detected over the time period that is studied.

To measure the variations of the activity A in space, we use the weighting W_Δ of the slip zone size (equation (9)). To measure the time variations, we use both the slip zone size weighting W_Δ and also the equal weighting W_0 of each event. The results are not affected by which weighting is used. To study the average behavior during a cycle between large events, we look at the activity as a function of the time before the large event and the distance from its epicenter. We then superimpose many of these cycles and measure an average weighted activity

$$\bar{A}(S,T) = \frac{1}{N_c}\sum_{n=1}^{N_c} A_W(s_n + S, t_n + T) \qquad (10)$$

where the integer n enumerates the loading cycles, N_c is the total number of cycles counted, s_n and t_n are the epicenter and occurrence time of the nth large event, and $t_{n-1} - t_n < T < 0$.

Numerically, we find that in the model the average activity is separable in the variables S and T. That is,

$$\bar{A}(S,T) = A_S(S)A_T(T)\ . \qquad (11)$$

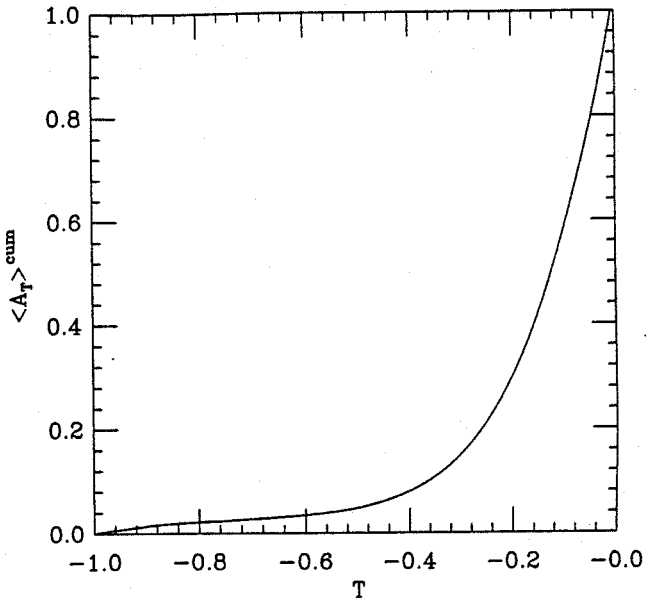

Fig. 4. The time dependence of the average cumulative activity per large event $< A_T >^{cum}$ versus T (equation(13)). T is measured in units of the average repeat time (equation(12)) of large events. The vertical axis is normalized so the cumulative activity at $T = 0$ is 1. Note the sharp turn-on of activity and steady increase up until the large event. The parameters used in this figure are $\alpha = 3$, $\xi = 6$, $\nu = 0.001$, and $N = 200$.

We look first at the variation of A_T and then at A_S.

The variation of the average activity in time is shown in Figure 4. We average over $N_c = 1000$ cycles and use the weighting W_Δ. The horizontal axis is the time T, measured in units of the average repeat time

$$\bar{t} = \frac{1}{N_c}\sum_{n=1}^{N_c} t_n - t_{n-1}\ . \qquad (12)$$

The large event happens at $T = 0$. On the vertical axis we plot the average cumulative time-varying activity per large event, $< A_T >^{cum}$:

$$< A_T >^{cum}(T) = \int^T \left[\frac{A_T(T')}{\int_{-\infty}^{T'} \rho(T'')dT''}\right] dT'\ . \qquad (13)$$

Since not all cycles have the same time between large events, we have divided by the fraction of events which have times between large events greater than T', $\int_{-\infty}^{T'} \rho(T'')dT''$, where ρ is the distribution of times between large events. This way, there is no increase in activity approaching $T = 0$ due to this distribution of times. We have also normalized $< A_T >^{cum}$ so its value at $T = 0$ is 1, since we are interested only in the variation of the activity. Examining the figure, we see a very low level of activity for the first two thirds of the cycle. At about one third of the average repeat time before the large event, there is a sharp, steady increase in the activity.

The increase in activity leading up to the large event (and the subsequent drop afterwards) is seen not only in an average sense but also for each individual cycle. A typical sequence of changes in activity is shown in Figure 5, where we plot the cumulative number of events as a function of time, in units of the average repeat time for large events. The times when the large events occur are marked by arrows and are seen to be associated with changes in the activity. In fact, we see essentially every drop in activity associated with

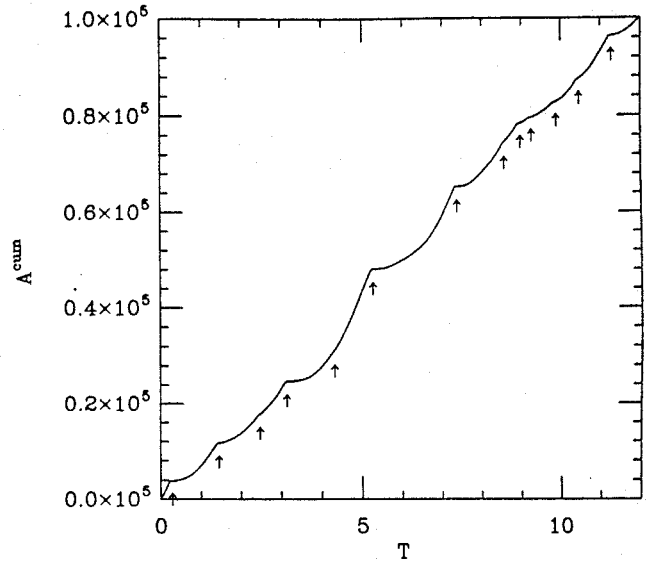

Fig. 5. Cumulative number of events as a function of time for a typical sequence of events in the model. Time is in units of the average repeat time for large events. The arrows correspond to times when large events occurred. Observe that nearly every drop in the activity (the slope of the curve) is associated with a large event, and, conversely, nearly every large event is associated with a drop in activity. The parameters used in this figure are $\alpha = 2.5$, $\xi = 6$, $\nu = 0.001$, and $N = 200$.

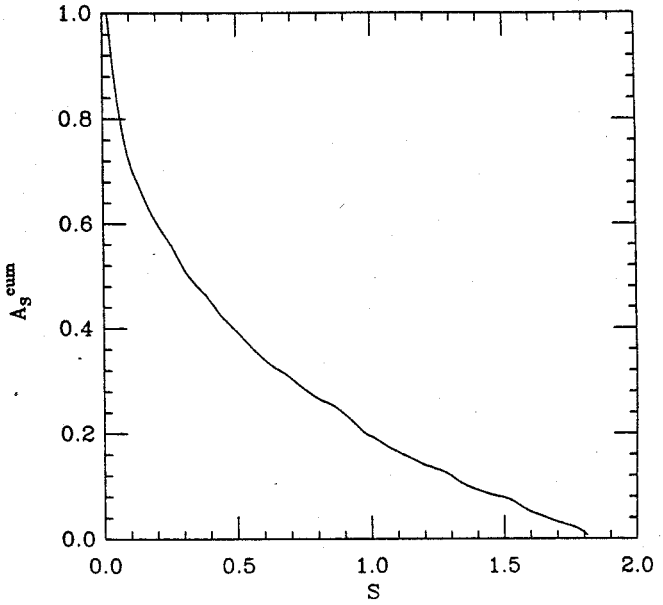

Fig. 6. The spatial distribution of the cumulative activity A_S^{cum} as a function of distance from the future epicenter of a large event, measured in units of $\tilde{\xi}$. We normalize the activity so the cumulative activity at the origin is 1. Note the strong maximum at the epicenter $S = 0$. The parameters used in this figure are $\alpha = 3$, $\xi = 6$, $\nu = 0.001$, and $N = 200$.

a large event, and, conversely, nearly every large event is associated with a drop in activity. We interpret the increase in activity as a precursor for large events. To see how this might be used in practice, note that for a given μ_{lower} and weighting W, there is an average cumulative activity per cycle. With this as a basis we set some cumulative activity threshold which is a small fraction of this average. Keeping track of the cumulative activity during a cycle, we can then monitor the time delay between when the cumulative activity crosses the threshold and when the large event occurs. Typically, this time delay is less than 20% of the large-event repeat time, when we set the threshold around a tenth of the average activity. This is a useful measurement in the model because of the sharp turn on in activity; one would need large activity variations in real earthquakes if it were to be useful there as well.

While these measurements reveal certain information regarding when a large event may be likely to occur, so far we have not found any correlations in our data which would allow us to predict how large it will be. The size of the upcoming event does not seem to be correlated with the cumulative activity, the activity rate, the time since the last large event, or the time since the onset of increased activity.

The variation of the average activity in space is shown in Figure 6. Here again we plot the cumulative activity on the vertical axis, this time integrating over space:

$$A_S^{\text{cum}}(S) = \int^S A_S(S')dS' \quad . \tag{14}$$

The horizontal axis is S measured in units of the delocalization length $\tilde{\xi}$ (equation (5)). The vertical axis is again normalized so the cumulative activity at the origin is 1. Note the sharp peak in activity at the epicenter of the forthcoming large event ($S = 0$).

The sharp increase in precursory activity near the epicenter, like the increase in the activity with time, occurs in the individual case as well as on average. Therefore the spatial variation can be used to predict the future epicenter. In Figure 7 we plot the position of the epicenter as a function of the position of the center of maximum activity for 1000 large events. To find the center of maximum activity, we measure the "neighboring activity" of a site by summing the activity at all sites within a distance $\tilde{\xi}/2$ on either side and then de-

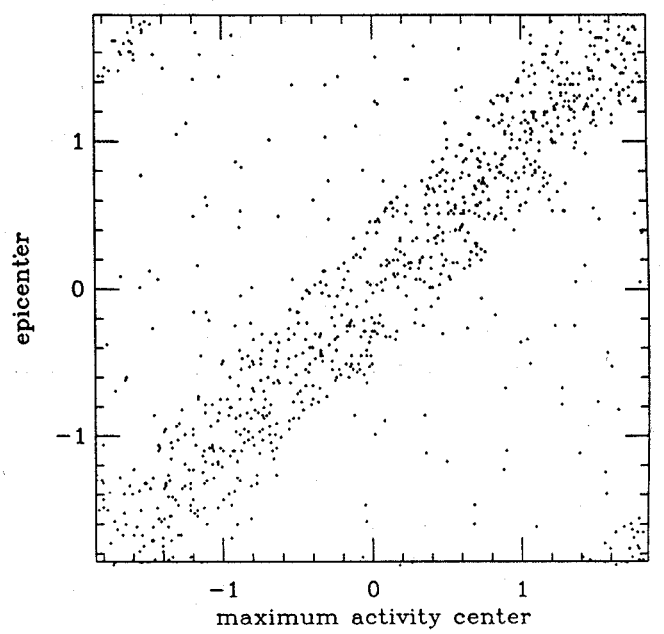

Fig. 7. The large-event epicenter versus the center of maximum previous activity, plotted in units of $\tilde{\xi}$. A 45° line stemming from the origin is the line of exact correspondence. Note that most of the points fall within $\tilde{\xi}/2$ of this line. Periodic boundary conditions are used, so the points at the upper left and lower right are close to the diagonal. The parameters used in this figure are $\alpha = 3$, $\xi = 6$, $\nu = 0.001$, and $N = 200$.

fine the center of maximum activity to be the site with the highest neighboring activity. We find that more than 80% of the events have their epicenters within $\tilde{\xi}/2$ of the center of maximum activity.

The correlation between increased small-scale activity and a future large event is a robust feature of this model. Perhaps the most important implication of this correlation — the one that seems most likely to persist in the real world — is that locally increased activity is nearly always a precursor to a large event. The converse of this statement seems less likely to be true. We can easily imagine adding to our model an extrinsic mechanism for locking the fault at some point, for example, by inserting a few blocks with anomalously large sticking friction. Then the activity of these blocks would remain small while stresses built up in their neighborhood, and the eventual slipping of this group of blocks would be likely to trigger a large event. In this case, a local precursory increase in activity would not be necessary for a large event; but such an increase would still be sufficient. That is, while a lack of activity in some regions is by no means an indication that nothing is about to happen, a rise in activity seems almost invariably to be a signal that stresses are rising toward a significant slipping point.

4. Patterns of Activity in Real Earthquakes

From the point of view of the model, we should search the catalogues to look for long term changes in activity and see whether or not they are followed by large events. This search is made difficult by the presence of aftershocks, which dramatically change to local rates of events. Instead, we will do a simpler study of looking at big events and the activity associated with their epicenters. The advantage of this approach is that it is a better defined study, and to some extent addresses the question of whether the increase in activity preceding large events seen in the model is also typically seen in the Earth. The disadvantage is that it does not address the main hypothesis, which is that large events need not be preceded by long-term increases in activity, but long-term increases in activity do signal a coming large event. We will do one case study where we look for long term increased activity in the San Francisco Bay Area, finding it on the central Calaveras fault, and argue that the Loma Prieta event was associated with that increase. We then turn to the question of whether this behavior is always seen: the answer will be no. We will see, however, that the different patterns that are seen are significant, in that they are characteristic of a given area, and repeatable for different events.

We now turn to real seismicity data for two regions in California. In this section we exclusively use the weighting W_0 (equation (8)) in which each event above a lower cutoff counts equally, regardless of magnitude. The lower cutoff is taken to be the local Richter magnitude M_L below which homogeneous data are not available. (By homogeneous data, we mean that within the time window we are considering, events at the lower-magnitude cutoff had an equal probability of being detected. This avoids the possibility that changes in instrumentation would affect the changes in activity we are examining.) The two data sets are $M_L > 2.5$ since 1948 for an inclined rectangular strip surrounding the San Andreas fault zone between 119° to 125° longitude and 35° to 40° latitude in the north, taken from the UC Berkeley catalogue, and $M_L > 3$ since 1932 between 114° to 122° longitude and 32° to 36.5° latitude in the south, taken from the Caltech catalogue. We look at the cumulative number of events versus time along different faults, and near the epicenters of relatively big earthquakes ($M_L > 5.5$ in the north, $M_L > 6$ in the south). We refer to these events as "big", as opposed to "large", for which we have reserved the technical meaning of magnitudes larger than $\tilde{\mu}$. (Rough estimates suggest this transition magnitude may be between 6 and 7 [*Carlson, et al.*, 1991]). The distinction between "big" and "large" events needs to be emphasized. Ideally, we would like to only study activity patterns prior to large events, as was done in the model. There are not enough large events in California, though, to restrict the study in this way. This suggests looking at faults from other parts of the world, where there are more data for large earthquakes. The advantage of California, however, is that it has the longest record for small earthquakes. Thus we use "big" earthquakes in this study. One must be careful in mixing "big" and "large" earthquakes, as large ones release significant amounts of strain, while smaller ones do not. One final comment on the analysis we will be doing in this section: We have been able to look at average properties in the model because of the large data set and the uniformity of underlying conditions. The sparse data set we had available for real earthquakes precluded a similar simple averaging. There is an additional point that must be treated carefully, when one is dealing with real data, and that is, What is one averaging over? It is important to be averaging over similar things. For example, if long-term activity changes are occurring on a loading time scale, then the loading rate of a given fault would need to be factored into the analysis. Thus one needs to do much more complicated analyses to properly average real data. We have chosen to do very simple analyses that would have robust results and that are very immediately related to the catalogues themselves. Our results would be a useful aid in deciding what regions and events could be averaged over.

We observe patterns of activity that are characteristic of a given area, which are repeatable for different big earthquakes within that area, but which vary between areas. We consider the possibility that the pattern of activity on the central Calaveras fault was a precursor to the 1989 Loma Prieta earthquake. We first present the evidence leading to this interpretation; then, we look at patterns of activity in other areas of the San Andreas fault system.

The northern data set is shown in Figure 8*a*. Figure 8*b* shows the main faults in this region, along with all the $M_L > 5.5$ events that have occurred since 1948. The various symbols will be explained shortly. We begin by studying the activity around the San Francisco Bay Area. In Figure 9 we plot the cumulative number of events for the northern data set for the region between 36.9° and 38.5° latitude for the San Andreas fault (SAF), Calaveras fault, and Hayward fault. (The 36.9° lower latitude was chosen to encompass the 1989 Loma Prieta event, which occurred at 37.0° latitude, while remaining sufficiently high in latitude, to avoid the numerous small events on the creeping section of the San Andreas fault just below.)

These fault subsets are shown in Figure 8*b*. We see there has been a regional increase in activity during the last decade. This increase has mostly occurred along the Calaveras fault; the Hayward and San Andreas faults had nearly constant activity. This points to an obvious weakness in our analysis if

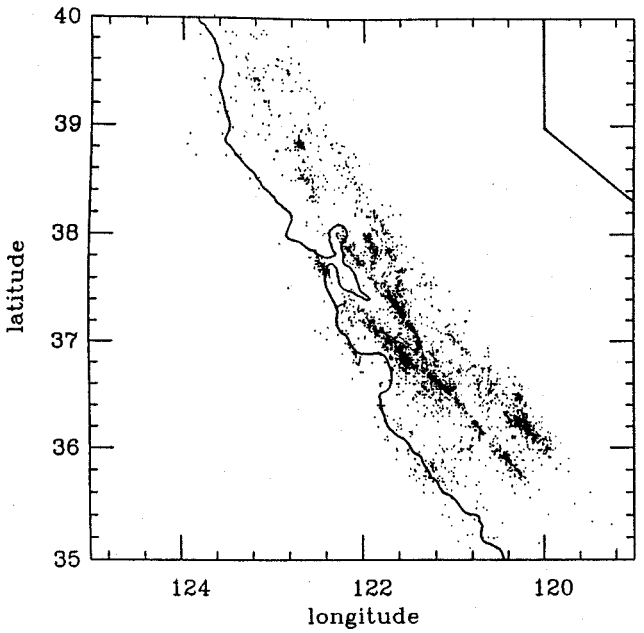

Fig. 8.*a* Map of seismicity in the region between 119° and 125° longitude and 35° and 40° latitude. Earthquakes with $M_L > 2.5$ since 1948 are marked by dots. The solid line is the coastline.

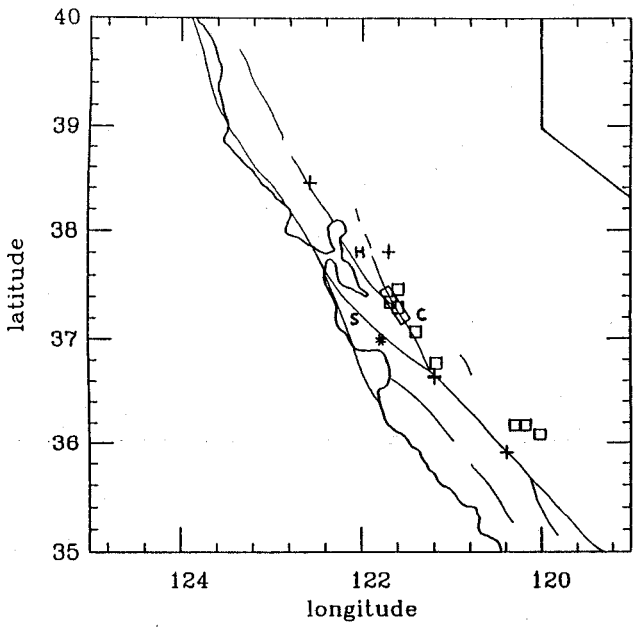

Fig. 8.*b* Map showing main faults and selected big earthquakes. The solid thick line is the coastline, and the thin lines are faults. The letters next to the faults denote faults referred to in the paper as follows: S, San Andreas; C, Calaveras; and H, Hayward. The symbols mark the epicenters of big ($M_L > 5.5$) earthquakes as follows: plus, activity returns to same rate after the big event as it had before; square, activity increases after the big event compared to before; asterisk, 1989 Loma Prieta M_L 7.0 earthquake. The rectangular box encloses the section of the Calaveras fault showing increased activity beginning in the 1980s.

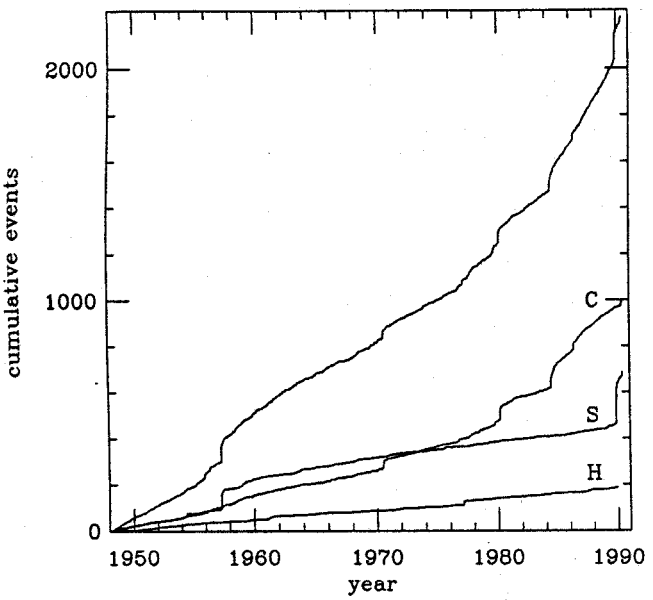

Fig. 9. The cumulative number of events as a function of time for various earthquake data sets in the San Francisco Bay Area between 36.9° and 38.5° latitude. The top curve is for the whole region. The curve marked *C* is for the Calaveras fault zone. The curve marked *S* is for the San Andreas fault. The curve marked *H* is for the Hayward fault. These faults are marked in Figure 8*b* with the same letters.

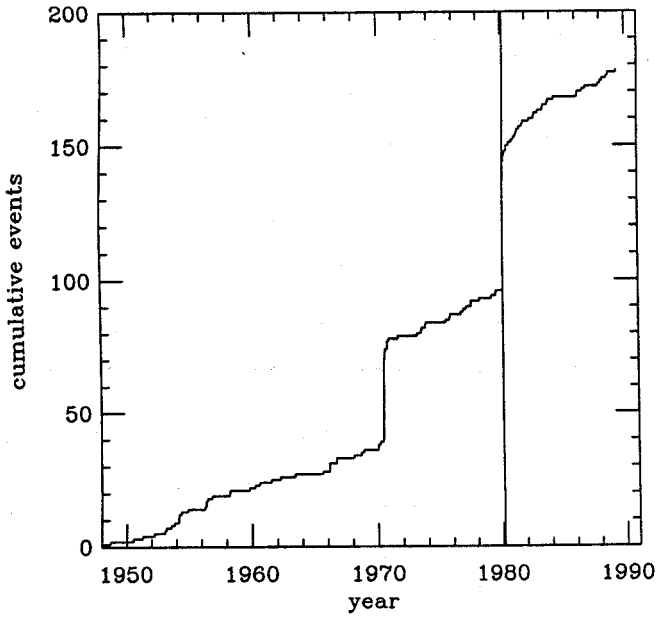

Fig. 10. The cumulative number of events as a function of time in a radius of 20 km surrounding the 1980 M_L 5.8 earthquake on the northern Calaveras fault. The activity appears to return to the same level after the big event as it had before the event. The vertical line marks the time of the 1980 earthquake. The step in the curve comes from the numerous aftershocks.

we are to interpret events in this region as belonging to distinct independent faults: we do not detect a significant signal on the SAF preceding the 1989 Loma Prieta earthquake.

There have been 15 $M_L > 5.5$ earthquakes in the northern region since 1948. These events are shown on the map in Figure 8*b*. The 1980 Livermore magnitude 5.8 earthquake occurred about 20 km to the east of the northern part of the Calaveras fault. The cumulative activity in a radius of 20 km (20 km equals the depth of strike-slip faults in California, and order of our estimates of $\tilde{\xi}$ for these faults. [*Carlson et al.*, 1991] around this earthquake is shown in Figure 10. The sharp steps in Figure 10 arise because of the tremendous number of aftershocks which accompany relatively big

events. Following a main event, the aftershock activity decreases steadily on a time scale which is much shorter than the time interval between large events. The aftershock period ends when the activity stabilizes or begins to rise. To obtain information which is pertinent to the next large event in a region, we must ignore the big steps in Figure 10, and instead pay attention to changes in the slope (i.e., Aw) of the cumulative activity curve. Observe that by 1985 the activity appears to have returned to its pre-1980 level. (Our discussion of patterns of activity in this paper is very qualitative. For more rigorous statistical methods, see, for example, *Reasenberg and Mathews* [1988].) This equality of the activity before and after a big earthquake is also seen in the pair of 1969 earthquakes that happened to the north near Santa Rosa. The epicenters of the six earthquakes showing this type of behavior are marked in Figure 8*b* with the plus symbol. This pattern contrasts markedly with all four big earthquakes along the central CFZ, where the activity increases after the big earthquakes. The 1979 magnitude 5.8 Coyote Lake earthquake, a clean example of this, is shown in Figure 11. The epicenters of these four earthquakes, and of the other three earthquakes showing this pattern of activity are marked by squares in Figure 8*b*. This increased activity is the signal we use as the basis of the forecast of a coming larger earthquake.

The increase in activity triggered by a big event may be the result of extrinsic inhomogeneities, or "asperities" [*Sykes*, 1983]. Breaking the asperity unlocks the fault and allows neighboring areas to move. While this type of behavior is beyond the homogeneous model we have studied, it is reminiscent of the way in which activity responds to the building stresses when the system gets near the time of the large event. We thus interpret the two patterns just described as follows: when the activity does not change following a big event, the system is not near the time of a large event, and when the activity does increase, the system is near the breaking threshold of a large event.

The epicenter of the 1989 Loma Prieta magnitude 7.0 earthquake is indicated by an asterisk in Figure 8*b*. Note that it is on the San Andreas fault opposite the region of increasing activity on the Calaveras fault, marked in Figure 8*b* by the rectangle, and that the separation between the faults at this point is only 30 km Did the Loma Prieta event unload the Calaveras fault? (For a discussion of stress changes produced by events on these neighboring faults on each other, see *Oppenheimer, et al.* [1988].) If significant stress has indeed been relieved on the Calaveras fault, we would expect that, after the aftershock activity has died down in the next few years, the activity level will drop down to, or below, the level it had in the 1950s. If this does not happen, there remains the possibility that the central section of the Calaveras fault will rupture. (There is, of course, other information seismologists use to estimate probabilities of various segments rupturing. Our intent here is to point out the implications of this particular feature.)

It is natural to ask whether there are other large earthquakes that have been preceded by the type of signal we have just pointed out, to see whether it is typical behavior or not. We have looked at the 16 $M_L > 6$ earthquakes that have occurred in southern California since 1942. The earthquakes having $M_L > 3$ since 1932 are shown in Figure 12*a*. The 16 $M_L > 6$ events, along with the main faults in this region, are

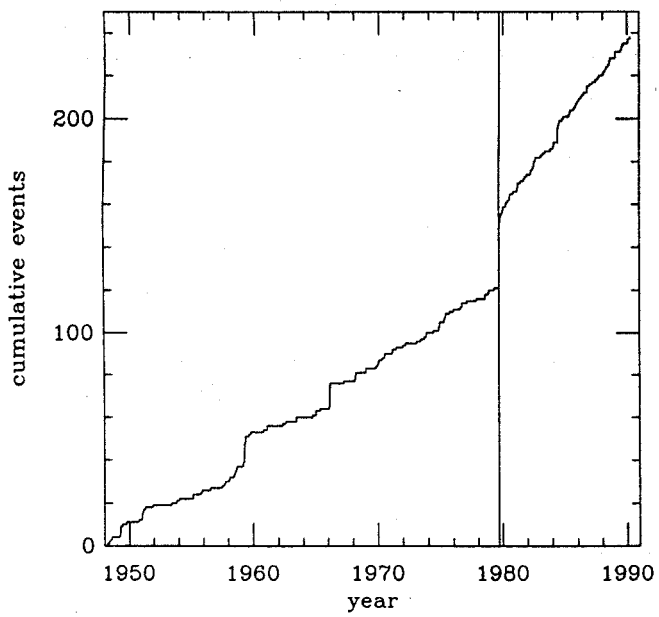

Fig. 11. The cumulative number of events as a function of time in a radius of 20 km surrounding the 1979 M_L 5.8 earthquake on the central Calaveras fault. The activity increases after the big event compared to before the event. The vertical line marks the time of the 1979 earthquake.

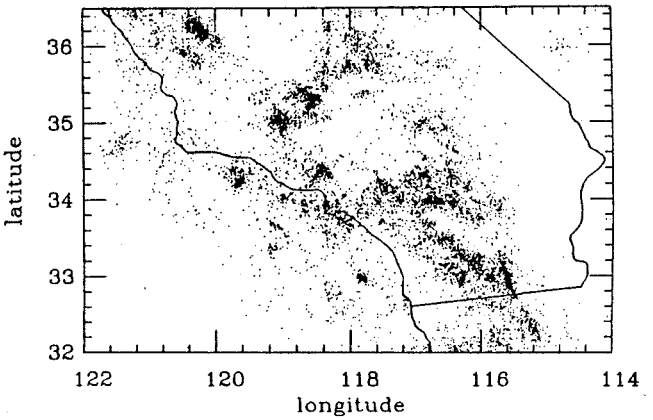

Fig. 12*a*. Map of seismicity in the region between 114° and 122° longitude and 32° and 36.5° latitude. Earthquakes with $M_L > 3$ since 1932 are marked by dots. The solid line encloses California and marks the coastline down through Mexico.

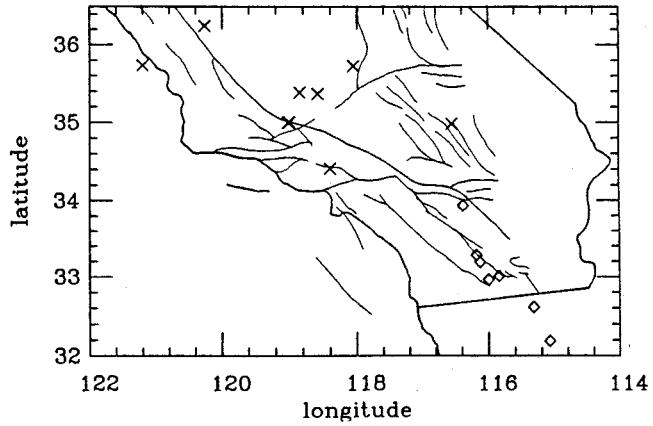

Fig. 12*b*. Map showing main faults and $M_L > 6$ earthquakes since 1942. The solid thick line encloses California and marks the coastline down through Mexico. The thin lines are faults. The symbols mark the epicenters of the big events as follows: crosses, there is little activity before the event, and decreasing activity, which we associate with aftershocks, extends over many years; diamonds, activity decreases after the big event compared to before, and aftershock activity ends in less than a couple of years.

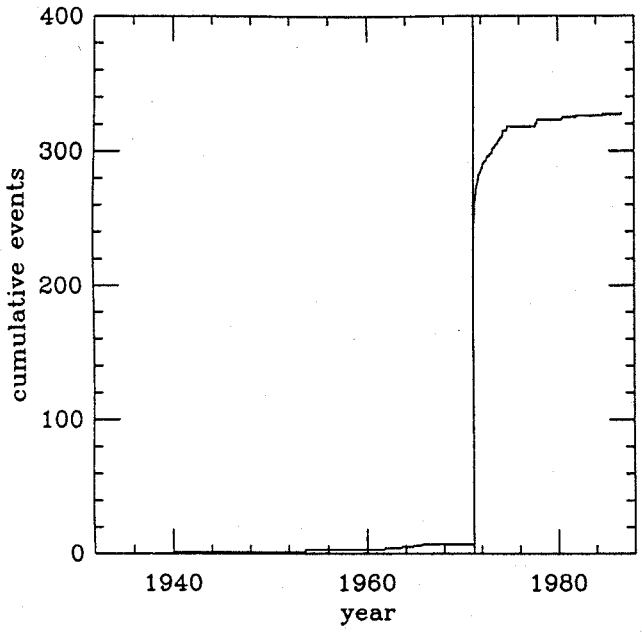

Fig. 13. The cumulative number of events as a function of time in a radius of 20 km surrounding the 1971 M_L 6.4 San Fernando earthquake in th e "big bend" area. There is very little activity preceding the big event, and a tail of aftershock activity extending many years. The vertical line marks the time of the 1952 earthquake.

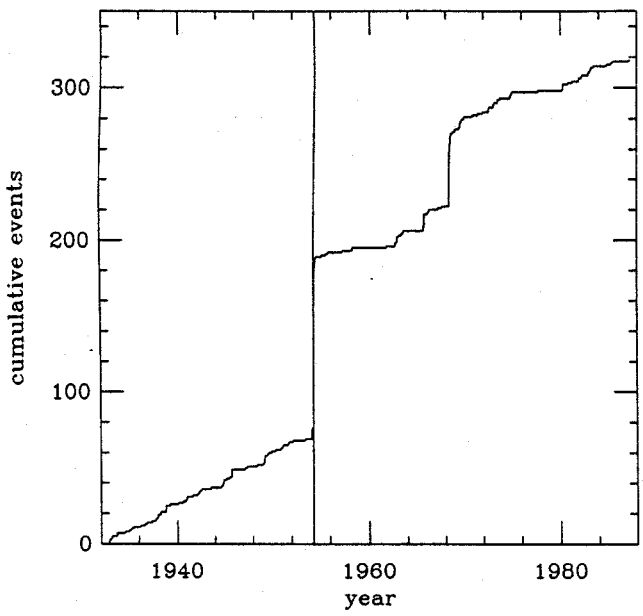

Fig. 14. The cumulative number of events as a function of time in a radius of 20 km surrounding the 1954 M_L 6.2 Arroyo Salada earthquake on the San Jacinto fault. There is also a M_L 6.4 event in 1968 inside the radius. In both cases, a decrease in activity follows the main event, as well as a rapid decay, compared to the "big bend" region, of aftershock activity. The vertical line marks the time of the 1954 earthquake.

marked in Figure 12*b*. The patterns of activity again show reproducibility for a given area for different earthquakes and variation between areas. Two main types of patterns are seen, neither of them the same as the one seen on the CFZ. The 1971 magnitude 6.4 San Fernando earthquake shown in Figure 13 is an example of the pattern of activity seen in the neighborhood surrounding epicenters of big earthquakes in the "big bend" area of the fault system north of Los Angeles. We see very little or no activity preceding the big earthquake, followed by long aftershock tails with activity decreasing over many years. The earthquakes showing this type of behavior are marked by crosses in Figure 12*b*; observe that they are all distributed to the north. The second type of pattern shows a decrease of activity following the big earthquake, with the time scale of the decay of the aftershock activity being at most a couple of years. An example of this pattern is the 1954 magnitude 6.2 Arroyo Salada earthquake shown in Figure 14. Earthquakes showing this pattern are marked by diamonds in Figure 12*b* and are seen to fall along the San Jacinto fault.

Can we understand these various activity patterns in the context of the model? The "big bend" pattern seems to require heterogeneities and the concept of locked faults, both outside the scope of the model so far. Of the patterns seen, the San Jacinto fault pattern seems closest to the pattern seen in the model. The geometry of the faults in these areas is consistent with this correspondence, as the model is meant to represent a single strike-slip fault. Of the fault zones we have considered so far, the San Jacinto fault is certainly closest to that geometry. While we do not fully understand any of these patterns, they do seem to be consistent with the main conclusions that we have drawn from the model. Increases in activity will not go away on their own; they are indicative of building stress near the threshold of a large event. Our belief is that not all large events will be preceded by long-term increases in activity, but, conversely, long-term increases in activity will be followed by large events. A systematic study of the catalogues to find significant long-term increases in activity that are not followed by large events would be an important disproof of this idea.

5. Conclusion

In the model, variations in the Gutenberg-Richter scaling exponent b are slight and not of use for predicting individual large events, while variations in the activity A are significant and potentially of predictive value. We find that A increases in time leading up to the large event and is largest in the neighborhood of the future epicenter. These features of the model, if also true for real earthquakes, would have a number of implications for interpreting patterns of seismicity.

The constancy of b suggests that looking only at relatively big events, or preshocks, may not be useful for predictive purposes. Changes in rates of these rarer big events are dominated by changes in A, so it is better simply to study variations in A, which are best determined by looking at smaller events.

The increase in A leading up to a large event is in direct conflict with the quiescence hypothesis, which suggests a decrease in activity prior to a large event. From cycle to cycle, A varies significantly in our simulations; but, within each cycle, we do not observe a drop in A prior to a large event. Similarly, our conclusion that the zone of maximum activity coincides with the zone where the large earthquakes are nucleated is in conflict with patterns like the "Mogi donut", which suggests a decrease in activity in the area surrounding the epicenter relative to the surrounding outlying activity [*Mogi*, 1969]. In order to see patterns like this, we believe that we would have to introduce extrinsic inhomogeneities into the model [*Kanamori*, 1981].

We have applied the idea of looking at variations in the activity to real earthquake data and found patterns of ac-

tivity that are the same for different earthquakes in a given area, but with different patterns in different areas. Not all large events are preceded by long-term increases in activity, but, we believe, long-term increases in activity are followed by large events. On the basis of an increase in activity beginning in the 1980s, we suggest the central section of the Calaveras fault may have been near the threshold for a large event. The 1989 Loma Prieta earthquake possibly has relieved the stress on the central Calaveras fault; in this case the seismicity pattern on this central section should change, with the activity decreasing to, or below, its level in the 1950s. If the activity remains high after a few years, the possibility remains that this section of the Calaveras fault will rupture. Activity in the next few years should help answer this question.

Could we have predicted the Loma Prieta event? Looking at the data up to the beginning of 1989, we have observed the signal for a coming large event on the c entral Calaveras fault. In contrast, the San Andreas fault exhibited a steady rate of activity for the preceding 20 years (see Figure 9). In 1989 a slight rise in activity on the San Andreas fault is detectable. This rise is not unprecedented on this fault: similar small but not persistent rises occurred in 1959 and 1963 without being followed by large events. However, at that time there was no signal on the Calaveras fault. Perhaps, then, a combination of the two signals could have been used this way: the long-term forecast of a large earthquake on the central Calaveras fault, along with close monitoring of nearby faults that could also be loaded by similar regional stresses. Unusual increases in activity on any of these faults could then signal a higher probability of rupture. (Similar techniques have been successfully used to predict earthquakes in a few cases. See, for example, *McNally* [1981].)

Acknowledgments. We benefited from numerous discussions with Craig Nicholson. We thank the Seismographic Stations of the University of California at Berkeley for the use of their data. This work was supported by NSF grant PHY89-04035, supplemented by funds from NASA, and by U.S. Department of Energy grant DE-FG03-84ER45108.

REFERENCES

Bak, P., C. Tang, and K. Wiesenfeld, Self-organized criticality: An explanation of $1/f$ noise, *Phys. Rev. Lett.*, *59*, 381, 1987.

Burridge, R., and L. Knopoff, Model and theoretical seismicity, *Bull. Seismol. Soc. Am.*, *57*, 341, 1967.

Carlson, J. M., Time intervals between characteristic earthquakes and correlations with smaller events: An analysis based on a mechanical model of a fault, to appear *J. Geophys. Res.*, *96*, 4255, 1991.

Carlson, J. M., and J. S. Langer, Properties of earthquakes generated by fault dynamics, *Phys. Rev. Lett. 62*, 2632, 1989*a*.

Carlson, J. M., and J. S. Langer, Mechanical model of an earthquake fault, *Phys. Rev. A 40*, 6470, 1989*b*.

Carlson, J. M., J. S. Langer, B.E. Shaw, and C. Tang, Intrinsic properties of a Burridge-Knopoff model of an earthquake fault, *Phys. Rev. A 44*, 884, 1991.

Davison, F. C., and C. H. Scholz, Frequency-moment distribution of earthquakes in the Aleutian arc: A test of the characteristic earthquake model, *Bull. Seismol. Soc. Am. 75*, 1349, 1985.

Gutenberg, B., and C. F. Richter, *Seismicity of the Earth and Related Phenomena*, Princeton University Press, Princeton, N.J., 1954.

Kanamori, H., The nature of seismic patterns before large earthquakes, in *Earthquake Prediction: An International Review, Maurice Ewing Ser., vol. 4*, edited by D. W. Simpson and P. G. Richards, p. 1, AGU, Washington, D.C., 1981.

McNally, K. C., Plate Subduction and Prediction of Earthquakes Along the Middle America Trench, *Earthquake Prediction: An International Review, Maurice Ewing Ser., vol. 4*, edited by D. W. Simpson and P. G. Richards, p. 63, AGU, Washington, D.C., 1981.

Mogi, K., Some features of seismic activity in and near Japan; activity before and after great earthquakes, *Bull. Earthquake Res. Inst. Univ. Tokyo 47*, 395, 1969.

Oppenheimer, D. H., P. A. Reasenberg, and R. W. Simpson, Fault plane solutions for the 1984 Morgan Hill, California, earthquake sequence: Evidence for the state of stress on the Calaveras fault, *J. Geophys. Res.*, *93*, 9007, 1988.

Reasenberg, P. A., and M. V. Mathews, Precursory seismic quiescence: A preliminary assessment of the hypothesis, *Pure Appl. Geophys. 126*, 374, 1988.

Schwartz, D. P., and K. J. Coppersmith, Fault behavior and characteristic earthquakes: Examples from the Wasatch and San Andreas fault zones, *J. Geophys. Res. 89*, 5681, 1984.

Smith, W. D., The b-value as an earthquake precursor, *Nature*, *289*, 136, 1981.

Sykes, L. R., Predicting great earthquakes, *Earthquakes: Observation, Theory and Interpretation, Proceedings of the Enrico Fermi International School of Physics*, edited by H. Kanamori and E. Boschi, North-Holland, Amsterdam, 398, 1983.

Wesnousky, S. G., C. H. Scholz, K. Shimazaki, and T. Matsuda, Earthquakes frequency distribution and the mechanics of faulting, *J. Geophys. Res. 88*, 9331, 1983.

Wyss, M., and R. E. Habermann, Seismic quiescence precursory to a past and a future Kurile Island earthquake, *Pure Appl. Geophys. 117*, 1195, 1979.

J.M. Carlson, Department of Physics, University of California, Santa Barbara, CA 93106.

J.S. Langer and B.E. Shaw, Institute for Theoretical Physics, University of California, Santa Barbara, CA 93106.

(Received November, 1990;
revised April 30, 1991;
accepted June 5, 1991.)